Available online at www.sciencedirect.com
ScienceDirect
Particuology 6 (2008) 390–403
PARTICUOLOGY
www.elsevier.com/locate/partic

Micromechanical investigation of granular ratcheting using a discrete model of polygonal particles

Fernando Alonso-Marroquín [a,*], Hans B. Mühlhaus [b], Hans J. Herrmann [c]

[a] *Earth Systems Science Computational Centre & School of Physical Sciences, The University of Queensland, Sta. Lucia, Qld 4068, Australia*
[b] *Earth Systems Science Computational Centre, The University of Queensland, Sta. Lucia, Qld 4068, Australia*
[c] *Institut für Baustoffe, ETH-Höenggerberg, Zürich, Switzerland*

Received 18 March 2008; accepted 15 July 2008

Abstract

We use a two-dimensional model of polygonal particles to investigate granular ratcheting. Ratcheting is a long-term response of granular materials under cyclic loading, where the same amount of permanent deformation is accumulated after each cycle. We report on ratcheting for low frequencies and extremely small loading amplitudes. The evolution of the sub-network of sliding contacts allows us to understand the micromechanics of ratcheting. We show that the contact network evolves almost periodically under cyclic loading as the sub-network of the sliding contacts reaches different stages of anisotropy in each cycle. Sliding contacts lead to a monotonic accumulation of permanent deformation per cycle in each particle. The distribution of these deformations appears to be correlated in form of vortices inside the granular assembly.

Keywords: Granular systems; Dynamics and kinematics of rigid bodies; Molecular dynamics methods

1. Introduction

1.1. What is ratcheting?

Chapter 46 of the Feynman Lectures on Physics (Feynman, Leighton, & Sands, 1963) contains a celebrated illustration of ratcheting device. As shown in Fig. 1, the ratchet consists of a pawl that engages the sloping teeth of a wheel, permitting motion in one direction only. In Feynman's ratchet, an axle connects this wheel with some vanes, which are surrounded by a gas. The vanes are randomly hit by the gas molecules, but due to the presence of the pawl, only collisions in one direction can make the wheel lift the pawl and advance it to the next notch.

The possibility to extract work from noise using such ratchet devices has attracted interest from many researchers (Howard, 1997; Reimann, 2002; Zapata, Bartussek, Sols, & Hänggi, 1996). Brownian motors, quantum ratchets or molecular pumps, all these machines operate under a similar ratcheting mechanism: the chaotic Brownian motion of the microworld cannot be avoided, but one can take advantage of it (Reimann, 2002). There is an extensive body of work on this subject, driven by the need to understand the molecular motors that are responsible for many biological motions, such as cellular transport (Svoboda, Schmidt, Schnapp, & Block, 1993) or muscle contraction (Kitamura, Tokunaga, Iwane, & Yanagida, 1999). Recently, this kind of mechanism has been experimentally demonstrated using the technology available to build micrometer scale structures. Many man-made ratchet devices have been constructed, and they are used as mechanical and electrical rectifiers (Reimann, 2002). Apart from these fascinating machines, the ratchet effect is used to describe economical or sociological processes where the intrinsic asymmetry in the system allows rectification of an unbiased input (Dybvig, 1995). In geological materials, ratcheting is a major cause of deterioration when the material is subjected to cyclic loading, thermal or mechanical fluctuations (Huang, Suo, Ma, & Fujimoto, 2000; Lekarp, Dawson, & Isacsson, 2000; Royer-Carfagni, 2004). An asymmetry in a foundation can produce tilting and eventual collapse of an engineering structure due to ratcheting (England, Tsang, Mihajlovic, & Bazaz, 1995). The tower of Pisa (Burland & Viggiani, 1994) is a well documented structure, where the tilt has been observed from its construction

* Corresponding author.
E-mail address: f.alonsomarroquin@uq.edu.au (F. Alonso-Marroquín).

1674-2001/$ – see inside back cover © 2008 Chinese Society of Particuology and Institute of Process Engineering, Chinese Academy of Sciences. Published by Elsevier B.V. All rights reserved.
doi:10.1016/j.partic.2008.07.015

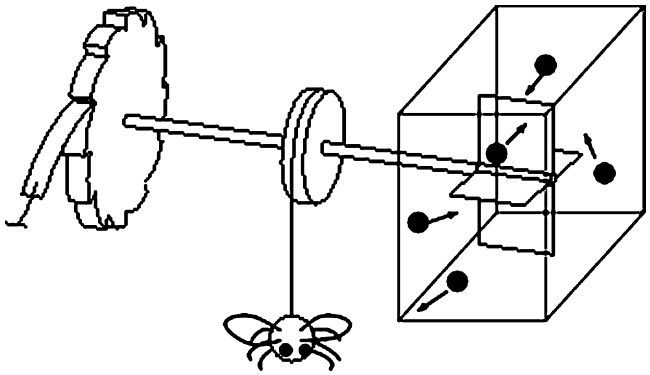

Fig. 1. Microscopic ratchet device introduced by Feynman et al. (1963). A wheel that can only turn one way is connected to a vane by an axle. The vane is inside a box with gas molecules in thermal equilibrium. Molecules randomly hit the vane. The sloping teeth of the wheel rectify the motion. The whole device converts random motion in work that can be used to lift a fly.

in 1174. Railway design is another important example. Granular materials are used as a supportive railbed. The excitations caused by trains induces permanent deformation in the granular bed (Lobo-Guerrero & Vallejo, 2006). Therefore a better understanding of the ratcheting response will reduce the maintenance cost of many engineering structures.

The existence of granular ratcheting as a long-time behavior in granular materials is still under discussion in the scientific and engineering community. This behavior refers to the constant accumulation of permanent deformation per cycle, when the granular sample is subjected to loading–unloading stress cycles with amplitudes well bellow the yield limit (Gudehus, 2006a). Ratcheting regimes are observed in both numerical (Alonso-Marroquin & Herrmann, 2004; David et al., 2005; Garcia-Rojo & Herrmann, 2005; García-Rojo, Alonso-Marroquin, & Herrmann, 2005; Peña et al., 2005) and physical (Lekarp et al., 2000; Triantafyllidis, 2004) experiments. There is no controversy about the existence of ratcheting when the stress amplitudes reach the yield criterion. However, it is not clear whether this effect persists for loading amplitudes well inside the yield surface, or whether there is a certain regime where no accumulation of deformation occurs. Numerical simulations have suggested that ratcheting may persist for loading amplitudes below the yield limit (Alonso-Marroquin & Herrmann, 2004; García-Rojo et al., 2005). Here we present a review of the ratcheting effect presented by the authors using polygonal packings (Alonso-Marroquin & Herrmann, 2004; Alonso-Marroquin, 2004). These results showed numerical evidence of granular ratcheting for small loading amplitudes in the quasistatic regime. We discuss here the microscopic origin of this effect, and its implications in soil mechanics and in the constitutive modeling of geomaterials.

This paper is organized as follows: in the present Section 1.1 we have introduced the concept of ratcheting. In Section 1.2 we introduce two different types of constitutive models (hypoplastic and elastoplastic models) for modeling cyclic loading. In Section 1.3 we summarize recent micromechanical observations showing deviations from the *classical* soil mechanics and supporting the existence of the granular ratcheting regime. Section 2 is devoted to modeling. In Section 3 we study the long-time, quasistatic strain response of a dense polygonal packing under cyclic loading. A micromechanical investigation of granular ratcheting in terms of induced anisotropy and deformation patterns is presented in Section 4.

1.2. Constitutive modeling

The modeling of the cyclic loading behavior of soils has been a central issue in the development of advanced constitutive equations. The 1960s have seen many significant developments in this field. Prior to this, soil mechanics was confined to linear elastic theory and the Mohr–Coulomb failure criterion. An important advance in the scope of soil plasticity occurred after the pioneering work of Roscoe and his coworkers in Cambridge, which led to the basic principles of the Critical State Theory (Roscoe & Burland, 1968; Wood, 1990). In an attempt to cover further aspects of cyclic soil behavior, subsequent developments have given rise to a great number of constitutive models (Gudehus, Darve, & Vardoulakis, 1984).

One important result of the theory of plasticity is the so-called *shakedown theory* (Hashiguchi & Chen, 1998; Lekarp & Dawson, 1998; Sharp & Booker, 1984; Werkmeister, Dawson, & Wellner, 2001). This theory predicts that a granular material accumulates plastic strains under cyclic loading if the magnitude of the applied load exceeds a threshold value called the shakedown limit. The material is then said to exhibit *incremental collapse* or *ratcheting*. If the loads are below this threshold, the accumulation of permanent deformation stops after a certain number of cycles. However, this basic assumption is difficult to verify by experiments on cyclic loading, because the onset of the ratcheting with the increase of the loading amplitude is gradual and not sharply defined (Werkmeister, Numrich, Dawson, & Wellner, 2002). This has motivated the development of the bounding surface model, where the elastic regime is shrunk to the current stress point (Dafalias, 1986).

The other approach to model soil behavior is the *black box* approach, in which the constitutive relation is derived by exploiting mathematical symmetries and representation theorems (Chambon, Desrues, Hammad, & Charlier, 1994; Kolymbas, 1993). The main advantage of this approach is that it offers a rigorous mathematical framework for the development of the tensor structure of constitutive relationships. Taking this perspective, some cyclic loading models have been developed starting from the theory of hypoplasticity (Kolymbas, 1993). This theory involves non-linear rate terms in order to capture the typical loading–unloading behavior of plastic deformation. Besides the stress and the void ratio, hypoplastic models introduce additional internal variables such as the back stress tensor (Kolymbas, Herle, & Wolfferdorff, 1995) or the intergranular strain (Niemunis & Herle, 1997). In order to give a physical basis to these internal variables, the concept of granular temperature has been introduced as a measure for velocity fluctuations of the grains (Jiang & Liu, 2007). However, the range of validity of statistical mechanics used in these approaches is still not fully resolved.

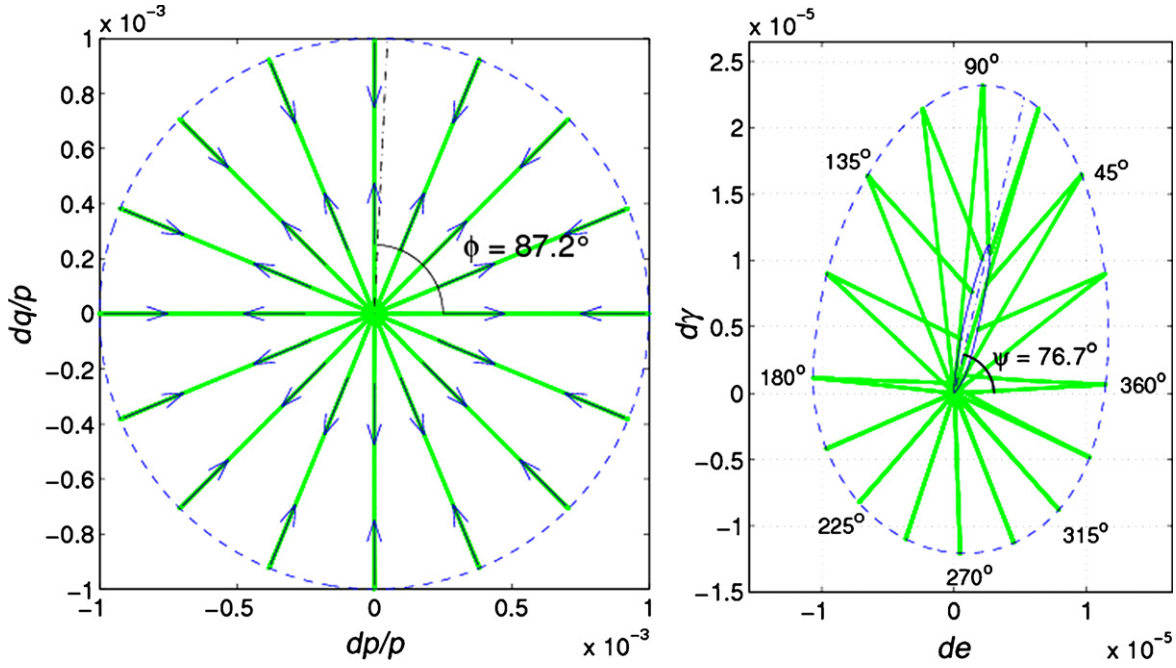

Fig. 2. Stress–strain relation resulting from the load–unload tests using a packing of polygons (Alonso-Marroquin & Herrmann, 2002). The stress components are the pressure $p = (\sigma_1 + \sigma_2)/2$ and the deviatoric stress $q = (\sigma_1 - \sigma_2)/2$. σ_1 and σ_2 are the principal components of the stress. The strain components are given by the volumetric de and the deviatoric $d\gamma$ part of the strain tensor. Grey solid lines are the paths in the stress and strain spaces. Grey dash-dotted lines represent the yield direction (left) and the flow direction (right). Dashed line shows the strain envelope response and the solid line is the plastic envelope response. The components of the initial stress state are $\sigma_1 = 1.25 \times 10^{-3}\, k_n$ and $\sigma_2 = 0.75 \times 10^{-3}\, k_n$. Here k_n is the normal stiffness at the contacts.

1.3. Micromechanical modeling

Most of the attempts to identify the internal variables of constitutive equations are based on macromechanical observations of the response of soil samples in conventional apparatus. A micromechanical investigation would help to select the physically motivated internal variables and to get insight into the principles and mechanics determining their evolution. After all, the mechanical response of granular soils is no more than a combined response of many micromechanical arrangements, such as interparticle slips, breakage of grains and wearing of the contacts. The development of micromechanical constitutive models is specially motivated by recent experiments on granular materials at grain scale (Majmudar & Behringer, 2005). Using photoelastic disks, these experiments show that stress in granular materials is transmitted through a heterogeneous contact network which reflects a broad contact force distribution. This broadness leads in turn to a considerable number of sliding contacts. These contacts are defined by the condition $|f_t| = \mu f_n$, where f_n and f_t are the normal and tangential contact force and μ the coefficient of friction. Under small deviatoric loads, an initially isotropic packing develops an anisotropic contact network because new contacts are created along the loading direction, while some contacts are lost perpendicular to it (Luding, 2004; Majmudar & Behringer, 2005; Madadi, Tsoungui, Lätzel, & Luding, 2004). Anisotropy is also observed in the sub-network of sliding contacts, because some contacts leave the sliding condition under slight deviatoric loading (Alonso-Marroquin, Luding, Herrmann, & Vardoulakis, 2005). Geometrical anisotropy leads to an anisotropic response of the granular assembly. The effect of the anisotropy of the contact network on the elastoplastic response has been recently investigated by the introduction of fabric tensors, measuring the orientational distribution of the contacts (Alonso-Marroquin et al., 2005).

The investigation of granular soils using particle-based simulations often involves oversimplified particle geometries and contact laws which are far from the properties of real soils. Nevertheless, these models are useful for identifying the role of induced anisotropy and the emergence of force chains in the elastoplastic response of these materials (Alonso-Marroquin & Herrmann, 2005; Pena, Lizcano, Alonso-Marroquin, & Herrmann, 2008). Despite their simplicity, particle-based models reproduce the complex structure of the incremental stress–strain response of granular materials (Alonso-Marroquin & Herrmann, 2005; Bardet, 1994; Calvetti, Viggiani, & Tamagnini, 2003; Kishino, 2003). These findings support attempts to base the construction of macroscopic constitutive relations on particle-based models. The particle models should capture realistic granulometric properties and interparticles interactions, and the constitutive models will describe the response of these particle models using incremental (or rate type) relations. The incremental relation can then be used in the Finite Element Codes for large-scale simulations.

The method of calculating the incremental response of particle-based models is the same as used soil mechanics (Gudehus, 1979; Poorooshasb, Holubec, & Sherbourne, 1967). This method has been implemented to calculate the incremental response of packings of disks (Bardet, 1994) and polygons (Alonso-Marroquin & Herrmann, 2002; Alonso-Marroquin et al., 2005). The incremental response in three-dimensional defor-

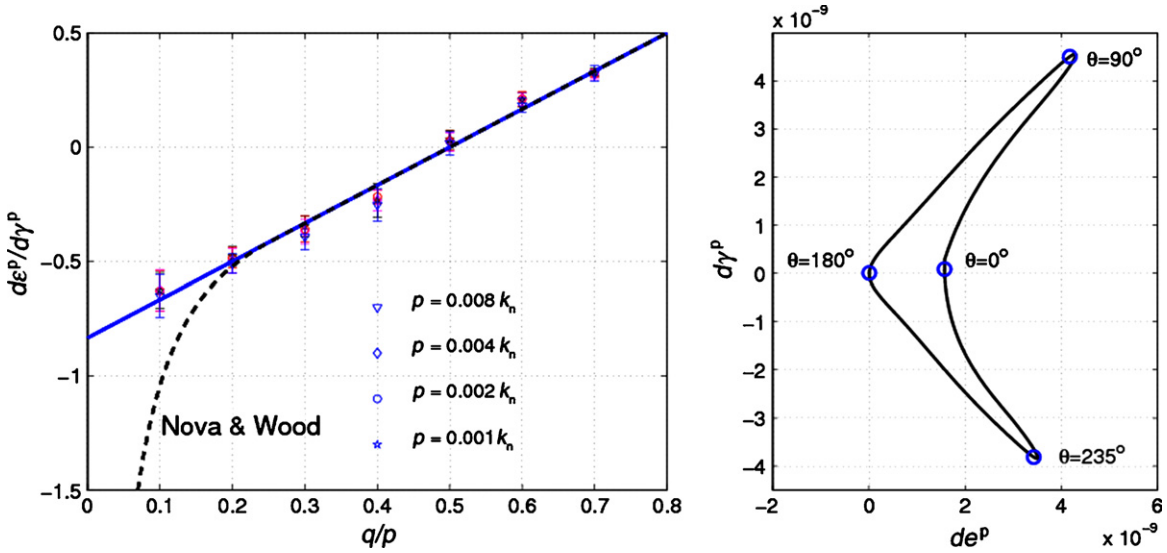

Fig. 3. *Left*: Dilatancy $d=-d\varepsilon^p/d\gamma^p$ versus the stress ratio $\eta=q/p$ obtained from the plastic incremental response of a polygonal packing (Alonso-Marroquin et al., 2005). The solid curve represents a linear fit; the dashed curve the relation given by the Nova and Wood model (Nova & Wood, 1979). *Right*: Plastic envelope response resulting from isotropically compressed polygonal packing with a pressure $p=0.001\,k_n$. Here k_n is the normal stiffness at the contacts.

mations has also been investigated using packings of spheres (Calvetti et al., 2003; Kishino, 2003). However, most of these calculations are still confined to plane strain deformation. In this case the stress space is completely described by the volumetric (p) and deviatoric (q) components of the stress. The incremental strain defines the strain space, whose components are the volumetric (de) and deviatoric ($d\gamma$) strain. The noncoaxiality angle, measuring the orientation of the principal direction of the strain with respect to the principal direction of the stress, is required for anisotropic materials (Alonso-Marroquin et al., 2005). The incremental response is given by a function between the incremental stress space and the incremental strain space.

Fig. 2 shows the typical incremental response resulting from a simulation using a perfect polygonal packing (Alonso-Marroquin & Herrmann, 2002). Starting from a point in the stress space, the packing is loaded using a specific direction and a fixed loading amplitude $\Delta\sigma=\sqrt{p^2+q^2}$. The end of the load paths in the stress space maps into a strain envelope response in the strain space. Then the sample is unloaded so that the sample returns to its original stress state. The corresponding strain point does not return to its initial state, so that the remaining strain corresponds to the plastic incremental strain. This procedure is implemented by choosing different stress directions with the same stress amplitude, so that the ends of the strain paths create the plastic part of the envelope response. As shown in Fig. 2, this envelope consists of a very thin ellipse, nearly a straight line, which confirms the unidirectional aspect of the irreversible response predicted by the elastoplasticity theory (Vermeer, 1984). The *yield direction* ϕ can be found from this response, as the direction in the stress space where the plastic response is maximal. In this example, this is around $\phi=87.2^\circ$. The *flow direction* ψ is given by the direction of the maximal plastic response in the strain space, which is around 76.7°. The fact that these directions do not agree reflects *a non-associated flow rule* that is also observed in experiments on realistic soils (Poorooshasb et al., 1967). From numerical simulations of packings of disks, Bardet (1994) concluded also that a non-associated flow rule describes satisfactorily the incremental response. This conclusion is also supported by several experimental tests on plane strain deformation (Nova & Wood, 1979; Vermeer, 1984; Wood, 1990). Both numerical and experimental results show clearly deviations from the normality condition. A possible reason for these deviations is that any load involves sliding contacts, so that the elastic regime is vanishing small, not a finite domain as the Classical Elastoplasticity assumes (Alonso-Marroquin & Herrmann, 2005). These results lead to the conclusion that a profound modification of elastoplasticity theory is required (Darve, Flavigny, & Meghachou, 1995).

Apart from the unidirectionality of the flow rule, simulations show that the dilatancy $d=-d\varepsilon^p/d\gamma^p$ and the stress ratio $\eta=q/p$ are related by the simple linear relation $d=c(\eta-M)$ (Fig. 3) (Alonso-Marroquin et al., 2005). This relation is not only supported by experiments, but it also has been one of the fundamental issues in modeling the stress–strain behavior of soils (Vardoulakis & Georgopoulos, 2005). A physical explanation of this relation is that the granular sample behaves like *a strange fluid* that obeys this stress–dilatancy relation as an internal kinematic constraint (Vardoulakis, 1983). This constraint becomes apparent near failure, where the plastic deformation dominates, and it could be seen as the counterpart of the well-known incompressibility condition of fluids. In this context, we should address the existing correlation between the mean orientation of the sliding contacts and the plastic flow direction (Alonso-Marroquin et al., 2005). This correlation suggests that this internal constraint can be micromechanically interpreted from the induced anisotropy of the sub-network of sliding contacts.

In the limit of small deviatoric loads, the kinematic constraint is no longer valid because elastic deformation dominates. However, the correlation between the stress–dilatancy relationship and the induced anisotropy is still valid (Alonso-Marroquin

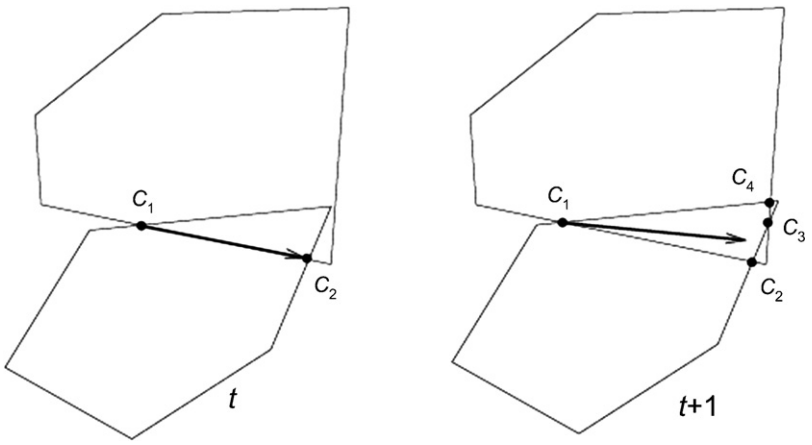

Fig. 4. Intersection points C_i before (left) and after (right) the formation of a pathological contact. The vector denotes the contact line and t represents the time step.

et al., 2005). Under extremely small deviatoric loads, some contacts depart from the sliding condition, leading in turn to anisotropy in the sub-network of the sliding contacts. The effect of this anisotropy on the plastic response becomes evident when we get the plastic envelope response of an isotropically compressed sample (see Fig. 3). Unexpectedly, the unidirectionality of the plastic deformations breaks down, because small deviatoric loads lead to deviatoric plastic deformations. This surprising effect contradicts the isotropic regimen postulated in several constitutive models (Nova & Wood, 1979).

We will study here how this plastic deformation evolves when an isotropically compressed sample is subjected to small cycles with deviatoric stress. We will see that the deviatoric strain increases as the number of cycles increases. A very surprising fact is that this accumulation does not stop for large number of cycles, but it grows linearly with respect of the number of cycles. We call his phenomena granular ratcheting.

2. Model

We use a particle-based model with polygonal particles to investigate granular ratcheting. The polygons are generated by Voronoi tessellation (Alonso-Marroquin & Herrmann, 2002). This method produces a range of areas of polygons following a Gaussian distribution with mean value ℓ^2 and variance of $0.36\ell^2$. The number of edges of the polygons is distributed between 4 and 8 for 98.7% of the polygons, with a mean value of 6. The interparticle forces include elasticity, viscous damping and friction with a sliding condition. The details of the interaction of the polygons will be presented in this section.

Defining contact forces between polygonal particles is far from a trivial task. A usual approach is to assume that the polygons cannot be deformed, but they can overlap when they are pressed against each other. Then the force is calculated as a function of this overlap (Kun & Herrmann, 1999; Tillemans & Herrmann, 1995). For the calculation of the contact force we require a well defined contact normal vector, which is perpendicular to the contact surface, and an overlapping length. The latter one measures the interpenetration between the two particles. It is desirable that these two quantities change continuously with time. Time discontinuities in the force eventually lead to numerical problems in the integration of the equation of motions, such as numerical generation of energy in the granular system.

The contact normal vector is taken perpendicular to the so-called *contact line*. This line represents the flattened contact surface between the two bodies in contact. We calculate the contact line from the intersection points of the overlapping polygons. In most cases, we have two intersection points, as shown in the left of Fig. 4. In such a case, the contact line is defined by the vector $\overrightarrow{C} = \overrightarrow{C_1C_2}$ connecting these two intersection points. In some pathological cases, the intersection of the polygons leads to four or six points. In these cases, we define the contact line by the vector $\overrightarrow{C} = \overrightarrow{C_1C_2} + \overrightarrow{C_3C_4}$ or $\overrightarrow{C} = \overrightarrow{C_1C_2} + \overrightarrow{C_3C_4} + \overrightarrow{C_5C_6}$, respectively. This choice guarantees a continuous change of the contact line, and therefore of the contact normal vector, during the evolution of the contact.

The contact force is decomposed as $\overrightarrow{f^c} = \overrightarrow{f^e} + \overrightarrow{f^v}$, where $\overrightarrow{f^e}$ and $\overrightarrow{f^v}$ are the elastic and viscous contribution. The elastic part of the contact force is decomposed as $\overrightarrow{f^e} = f_n^e \hat{n}^c + f_t^e \hat{t}^c$, where f_n^e is the normal elastic force and f_t^e is the frictional force. The calculation of these components is explained below. The unit tangential vector is defined as $\hat{t}^c = \overrightarrow{C}/|\overrightarrow{C}|$, and the normal unit vector $\hat{n}^c$ is taken perpendicular to $\overrightarrow{C}$. The point of application of the contact force is taken as the center of mass of the overlapping polygon.

As opposed to the Hertz theory for round contacts, there is no exact way to calculate the normal force between interacting polygons. Tillemans and Herrmann (1995) proposed to calculate this force as $f_n^e = -k_n A/L_c$ where k_n is the normal stiffness, A is the overlapping area and L_c is the characteristic length of the polygon pair. Our choice of L_c is $1/2(1/R_i + 1/R_j)$ where R_i and R_j are the radii of the circles of the same area as the polygons. This normalization is necessary to be consistent in the units of force. Since the overlapping area changes continuously with time, the normal elastic force is continuous too.

The frictional force is calculated using a variation of the Cundall–Strack methods (Cundall & Strack, 1979). An elastic force $f_t^e = -k_t \Delta x_t$ proportional to the elastic displacement is included at each contact. k_t is the tangential stiffness. In order to satisfy the sliding condition $|f_t^e| < \mu f_n^e$, the elastic displace-

ment Δx_t is calculated as follows: when two particles come into contact we set $\Delta x_t = 0$. Then, at each time t, we guess a new value for the tangential elastic deformation as

$$\Delta x_t^p(t) = \Delta x_t(t - \Delta t) + v_t^c \, \Delta t, \tag{1}$$

where v_t^c is the tangential component of the relative velocity at the contact:

$$\vec{v}_t^c = \vec{v}_i - \vec{v}_j + \vec{w}_i \times \vec{l}_i - \vec{w}_j \times \vec{l}_j. \tag{2}$$

$\vec{v}_i$ is the linear velocity and $\vec{w}_i$ is the angular velocity of the particles in contact. $\vec{l}_i$ is the so-called *branch vector*, which connects the center of mass of the particle to the center of mass of the overlapping polygon. The predicted value of elastic deformation is corrected to satisfy the Coulomb sliding condition:

$$\Delta x_t(t) = \text{sign}(\Delta x_t^p(t)) \min\left(\frac{\mu k_n \, \Delta x_n(t)}{k_t}, |\Delta x_t^p|\right). \tag{3}$$

It has been shown that this frictional force reproduces the main features of the plastic deformation of soils, such as the plastic flow rule (Alonso-Marroquin et al., 2005), the stick-slip fluctuations (Alonso-Marroquin, Vardoulakis, Herrmann, Weatherley, & Mora, 2006; Pena et al., 2008) and ratcheting (Alonso-Marroquin & Herrmann, 2004). The main drawback of this method is that it introduces an time integration error of $O(\Delta t^2)$. Improvement of the calculations of such frictional force will require higher order integration terms in Eq. (1).

Finally, we introduce a viscous force (Eq. (4)), which is necessary to maintain the numerical stability of the method and to obtain a quick convergence to the equilibrium configuration.

$$\vec{F}_v^c = -m(\gamma_n \cdot \vec{v}_n^c \cdot \hat{n}^c - \gamma_t \cdot \vec{v}_t^c \cdot \hat{t}^c), \tag{4}$$

where $m = (1/m_i + 1/m_j)^{-1}$ is the effective mass of the two particles in contact, γ_n and γ_t are the damping coefficients. These forces introduce time dependent effects during the loading. However, it was shown that these effects can be arbitrarily reduced by increasing the loading time, as corresponds to the quasistatic approximation.

The transmitted torque between two polygons in contact is calculated as $\vec{\tau} = \vec{\ell} \times \vec{f}$. Since the point of application of the force is not collinear with the centers of masses of the interacting polygons, there is a contribution of the torque from both components of the contact force. This makes an important difference with respect to the interaction between disks or spheres: polygons can transmit torques even in absence of frictional forces.

The evolution of the position $\vec{x}_i$ and the orientation φ_i of the polygon i is governed by the equations of motion:

$$\begin{aligned} m_i \ddot{\vec{x}}_i &= \sum_c \vec{f}_i^c + \sum_b \vec{f}_i^b, \\ I_i \ddot{\varphi}_i &= \sum_c \vec{\ell}_i^c \times \vec{f}_i^c + \sum_b \vec{\ell}_i^b \times \vec{f}_i^b. \end{aligned} \tag{5}$$

Here m_i and I_i are the mass and moment of inertia of the polygon i. The first sum goes over all those particles in contact with this polygon; the second one over all the forces applied on the boundary of the assembly. We use a fifth-order Gear predictor-corrector method for solving the equation of motion (Allen & Tildesley, 1987).

Table 1
Parameters of the simulations.

Symbol	Default value	Parameter
k_n	1.6×10^8 N/m	Normal contact stiffness
k_t	0.528×10^8 N/m	Tangential contact stiffness
μ	0.25	Friction coefficient
γ_n	4×10^3 s^{-1}	Normal coefficient of viscosity
γ_t	8×10^2 s^{-1}	Tangential coefficient of viscosity
γ_b	4×10^1 s^{-1}	Coefficient of viscosity of the walls
t_0	0.1 s	Time of load
Δt	2.5×10^{-6} s	Time step for the molecular-dynamics
ρ	1 g/cm^2	Density of the grains
ℓ	1.0 cm	Size of the cells of the Voronoi generation
p_0	1.6×10^5 N/m	Confining pressure

There are many parameters in the simulation. The contact stiffnesses and the coefficient of friction define two important material parameters of the model: the ratio between the tangential and normal contact stiffnesses is $k_t/k_n = 0.33$, and the friction coefficient is $\mu = 0.25$. The other parameters are chosen to keep the stability of the numerical model and to guarantee quasistatic deformation. A list of the parameters is included in Table 1.

3. Granular ratcheting

Simulations are performed using five different samples. Each sample consists of 400 polygons, which are packed in the following way: first, the polygons are placed randomly inside a rectangular frame consisting of four walls. Then, a gravitational field is applied and the sample is allowed to consolidate. The external load is imposed by applying a force $\sigma_1 H$ and $\sigma_2 W$ on the horizontal and vertical walls, respectively. Here σ_1 and σ_2 are the vertical and horizontal stresses. H and W are the height and the width of the sample. The polygonal packing is isotropically compressed until the pressure p_0 is reached. When the velocity of the polygons vanishes gravity is switched off. Then, the vertical stress $\sigma_1 = p_0$ is kept constant and horizontal stress is modulated as

$$\sigma_2 = \frac{p_0 + \Delta\sigma[1 - \cos(\pi t/t_0)]}{2}, \tag{6}$$

with $\Delta\sigma$ being the loading amplitude and t_0 the period of each cycle.

3.1. Stress–strain relation

The strain tensor is calculated as the symmetric part of F_{ij}, where F_{ij} is the average of the gradient of the displacement field over a representative element volume (RVE). This volume consists of the space occupied by all the particles whose distance from the center of the assembly is less than 10ℓ. The exact expression of the averaged displacement field over the (RVE) can be found in Alonso-Marroquin & Herrmann (2005). From the eigenvalues ε_1 and ε_2 of the symmetric part of the strain tensor we obtain the deviatoric strain as $\gamma = \varepsilon_1 - \varepsilon_2$. The volume fraction is calculated as $\Phi = (V_p - V_0)/V_b$, where V_p is the sum

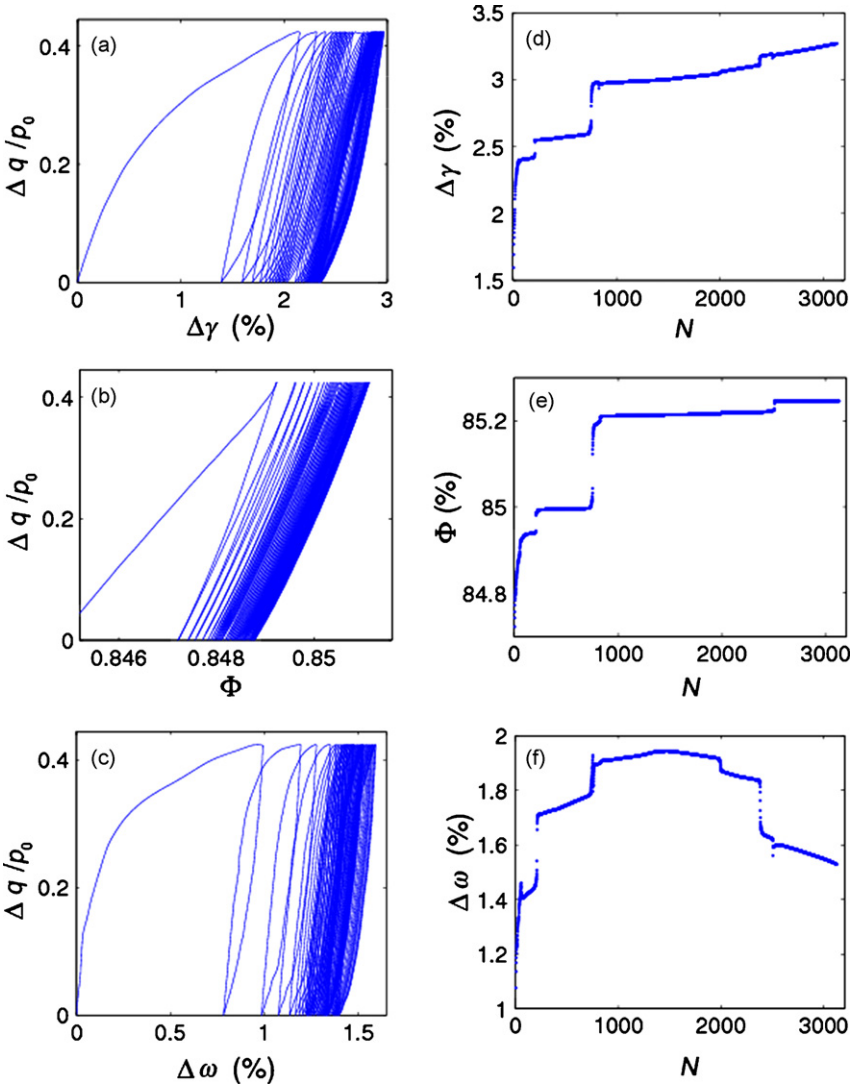

Fig. 5. Stress–deformation relation in a polygonal packing subjected to cyclic loading: (a) deviatoric stress versus deviatoric strain in the first 40 cycles; (d) permanent (plastic) strain γ_N after N cycles versus the number of cycles; (b) stress against the volume fraction in the first 40 cycles; (e) volume fraction Φ_N after N cycles versus number of cycles; (c) stress against vorticity $\Delta\omega$; (f) vorticity after N cycles versus number of cycles.

of the areas of the polygons, V_0 the sum of the overlapping areas between them, and V_b the area of the rectangular box. The vorticity is calculated as the antisymmetric part $\omega = (F_{12} - F_{21})/2$ of F_{ij}.

Fig. 5(a) shows the relation between the stress $q = (\sigma_1 - \sigma_2)/2$ and the shear strain γ in the case of a loading amplitude $\Delta\sigma = 0.424\,p_0$. This relation consists of open hysteresis loops which narrow as consecutive load–unload cycles are applied. This hysteresis produces an accumulation of strain with the number of cycles which is represented by γ_N in Fig. 5(d). We observe that γ_N consists of short time regimes, with rapid accumulation of plastic strain, and long time *ratcheting regimes*, with a constant accumulation rate of plastic strain of around 10^{-6} per cycle.

The relation between the stress and the volume fraction is shown in Fig. 5(b). This consists of asymmetric compaction–dilation cycles leading to compaction during cyclic loading. This compaction is shown in Fig. 5(e). We observe a slow variation of the volume fraction during the *ratcheting* regime, and a rapid compaction during the transition between two ratcheting regimes. The slope of γ_N shows no dependency on the compaction level of the sample. The evolution of the volume fraction seems to be rather sensitive to the initial random structure of the polygons. Even so we found that after 3×10^3 cycles the volume fraction still slowly increases in all the samples, without reaching a saturation level.

Vortices contribute substantially to global deformation, as shown in Fig. 5(c). We observe clockwise vorticity in the loading stage, followed by counterclockwise vorticity in the unloading stage. Vorticity also changes drastically during the transition between two ratcheting regimes, as shown in Fig. 5(f). The vorticity evolves slowly during ratcheting regimes; and rapidly during the transition between two ratcheting regimes. A non-monotonic behavior is observed in the time evolution of this vorticity field. This behavior is not affected by the compactification level of the sample.

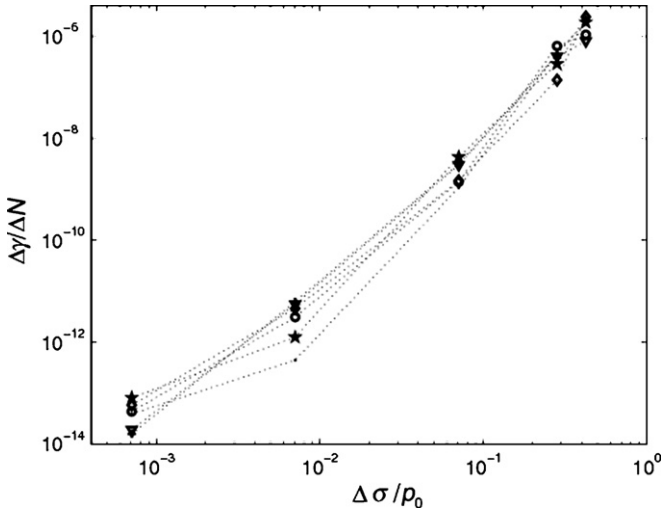

Fig. 6. Permanent deviatoric deformation per cycle versus loading amplitude in the ratcheting regime. The calculations are performed on six different polygonal samples (Alonso-Marroquin & Herrmann, 2004).

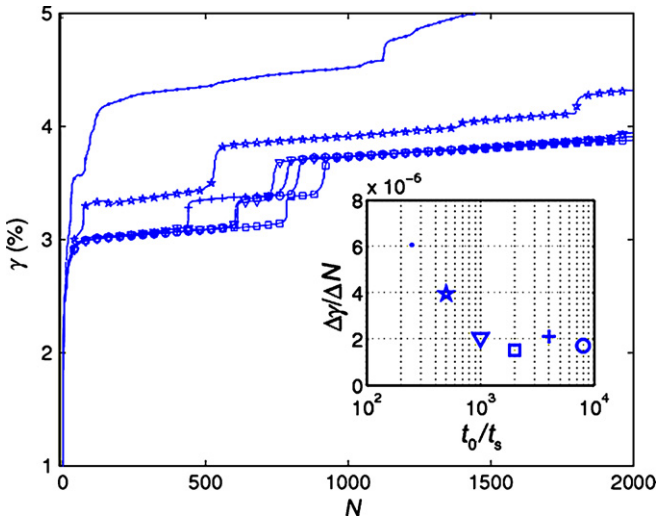

Fig. 7. Permanent deviatoric strain versus the number of cycles for different periods t_0 of cyclic loading. The inset shows the plastic deformation per cycle averaged over the last 1000 cycles. Each symbol in the inset corresponds to a value of t_0/t_s, where $t_s = \sqrt{m/k_n}$, with m being the averaged mass of the polygons, and t_0 is defined in Eq. (6).

One would expect that for small enough loading amplitudes, one can reach the elastic regime postulated in the shakedown theory (Sharp & Booker, 1984). In an attempt to detect this elastic regime, we decreased the amplitude of the load cycles and evaluated the corresponding asymptotic response of the deviatoric plastic strain. During the first stage of cycles a transient regime showing a decay of the permanent deformation per cycle is observed. However, after some hundred cycles, the sample reaches an asymptotic limit, where the plastic deformation in each cycle becomes constant. Regardless of the amplitude of the loading cycles, one always obtains ratcheting behavior in the long time limit. This is shown in the accumulation strain rate $\Delta\gamma/\Delta N$ for different loading amplitudes $\Delta\sigma$ in Fig. 6. A constant accumulation of strain is observed during cyclic loading, even when the amplitude is as small as 10^{-3} times the applied pressure. Of course, due to the smallness of the ratcheting response for these loading amplitudes, one can say that for small loading amplitudes the response is practically elastic. Even the slight repeated loading produced by transit of ants would produce plastic deformation after some centuries. However it is not possible to make them to follow the same path all this time. However, it is important to note that Fig. 6 shows a smooth transition from the shakedown response to the ratcheting response. This means that the transition from ratcheting to shakedown regime is too smooth that it does not allow identification of a purely elastic regime.

In view of the extremely small strain levels accumulated during the cycling loading, one would doubt that the simulations really capture the physical origin of the phenomenon. In the simulation extremely small changes are involved, so that the influence of time discretization and the floating point errors on results can be important and accumulative as a large number of iterations are involved. To reduce the discretization error, we choose a fourth order predictor–corrector algorithm as the integrator scheme. The time step is chosen by performing a set of simulations with 2000 loading cycles with different time step values. Then we found an error in the permanent deformation per cycle lower than 3% when the time step lower than $\Delta t = 0.15\sqrt{m/k_n}$, where m is the minimal mass of the particles and k_n is the contact stiffness. Then we choose $\Delta t = 0.1\sqrt{m/k_n}$.

There are also errors given by the floating point precision of the processor. Even with double precision, the errors (for addition/subtraction of floating point numbers) lies on the order of about 10^{-7} on a computer. These errors are evaluated by running the same simulations using two different compilers. Comparing the plastic deformation per cycle in both simulations, we found a discrepancy of 1.7%. Therefore we have no reason to believe that the ratcheting comes from a cumulative systematic error of the numerical method.

Another important question is whether ratcheting is a genuine quasistatic effect. Since the equations of motion include damping forces and inertia terms, it is important to know their role in granular ratcheting. Damping and inertial effects can be evaluated by performing the same test with different loading frequencies. Fig. 7 shows that as the frequency is reduced, the ratcheting tends to a constant value. From this result one can conclude that damping or inertial effects do not affect the appearance of ratcheting in the sample, so that this is a purely quasistatic effect.

4. Micromechanics of granular ratcheting

The existence of ratcheting for extremely small loading amplitudes appears to be somewhat counter-intuitive. First, from the classical theory of elastoplasticity one would expect a certain regime where only reversible deformation is possible. Second, our discrete model does not incorporate wearing of the grains. In practice, abrasion at the contacts leads to progressive rounding of the grains, which explains the accumulation of plastic deformation under cyclic loading (Festag, 2003). Nevertheless, we

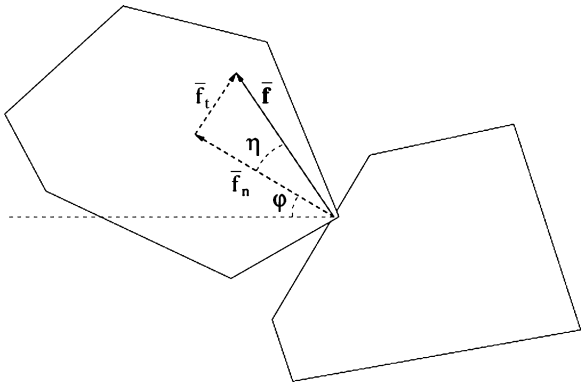

Fig. 8. Relevant variables of the contact force $\vec{f}$. This is decomposed into a normal $\vec{f}_n$ and a tangential $\vec{f}_t$ component. The orientation angle φ is the direction of the normal force. The mobilized angle η satisfies $\eta = \arctan(|\vec{f}_t|/|\vec{f}_n|)$.

will see that the dynamics of the contact network can explain how ratcheting evolves in samples with constant granulometric properties.

Each contact is characterized by the variables shown in Fig. 8. The contact force $\vec{f}$ is decomposed into its normal $\vec{f}_n$ and tangential $\vec{f}_t$ components with respect to the contact surface. The angle φ is the orientation of the normal force. The mobilized angle $\eta = \arctan(|\vec{f}_t|/|\vec{f}_n|)$ allows us to distinguish between sliding and non-sliding contacts. The sliding condition is given by $\tan(\eta) = \pm\mu$, where μ is the coefficient of friction.

4.1. Contact network

A striking feature of granular materials is the convoluted heterogeneous structure of the contact forces. As shown in Fig. 9, the stress applied on the boundary of the assembly is transmitted through force chains along which the contact forces are stronger than on average. Force chains lead to a wide distribution of the contact forces in both the tangential and normal directions.

We first study the evolution of the distribution of the normal forces $\vec{f}_n$ and mobilized angle η during cyclic loading. A broadening of the distribution is observed during each loading phase, followed by a narrowing of the distribution during the unloading phase. When the ratcheting regime is reached, the time evolution of this distribution is characterized by a broadening phase followed by a narrowing one in each cycle. In the ratcheting regime, this distribution shows a periodic broadening–narrowing regime.

To demonstrate this periodicity, the distribution of normal forces and mobilized angles at different snapshots of the simulation is plotted in Fig. 10. Note that although all distributions were measured at different times of the simulation, they correspond to the same stage of the cyclic loading. The shape of the distribution at this point remains approximately constant throughout the whole simulation. The contact force distribution evolves almost periodically during the cyclic loading. We also observe a peak in the distribution of mobilized angle at $\eta = \mu = 0.25$. This peak suggests that an important number of contacts reach periodically the sliding condition during the ratcheting regime. An important issue in the granular ratcheting is the orientational distribution of these sliding contacts, which is studied in the next section.

4.2. Anisotropy of the sliding contacts

The anisotropy of the granular sample can be characterized by the orientational distribution of the normal forces. For small deviatoric loads (i.e. $\Delta\sigma < 0.5\Delta\sigma_{\max}$, where $\Delta\sigma_{\max}$ is the peak value), anisotropy in the contact network is almost absent, and the coordination number of the packing keeps approximately its initial value $N_0 \approx 4.4$ in all the simulations.

The onset of anisotropy is different if one considers only the sliding contacts. These contacts play an important role, because they carry most of the irreversible deformation of the granular assembly during the cyclic loading. This anisotropy is described by the polar function $\Omega^s(\varphi)$, where $\Omega^s(\varphi)\Delta\varphi$ is the number

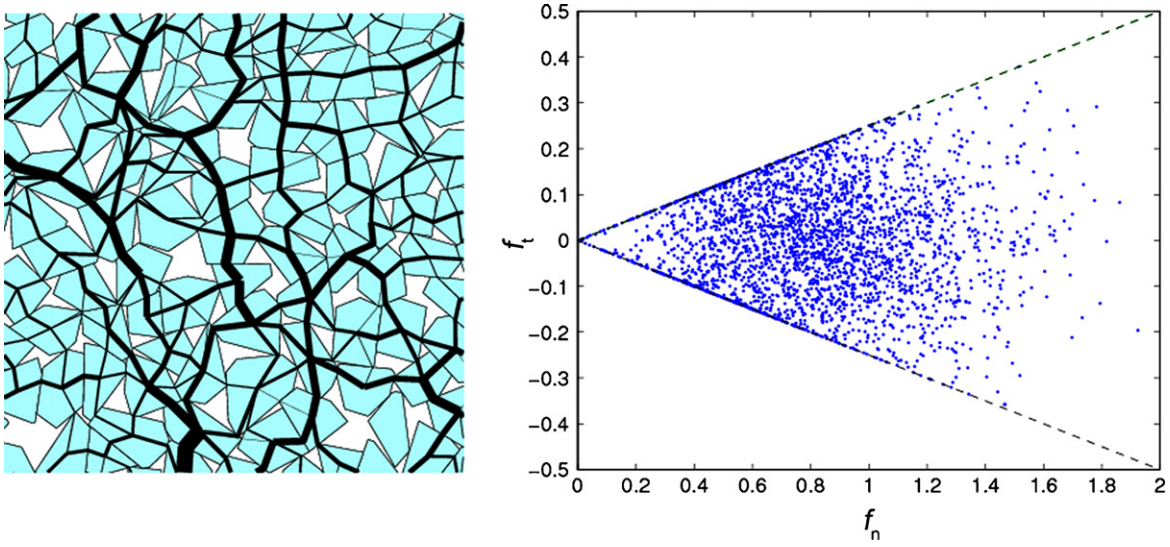

Fig. 9. *Left*: Contact force network in an isotropically compressed sample. The width of the lines represents the magnitude of the normal force. *Right*: Distribution of contact forces. Each point represents the normal and tangential component of the contact force. Dashed lines represent the sliding condition $|\vec{f}_t| = \pm\mu|\vec{f}_n|$.

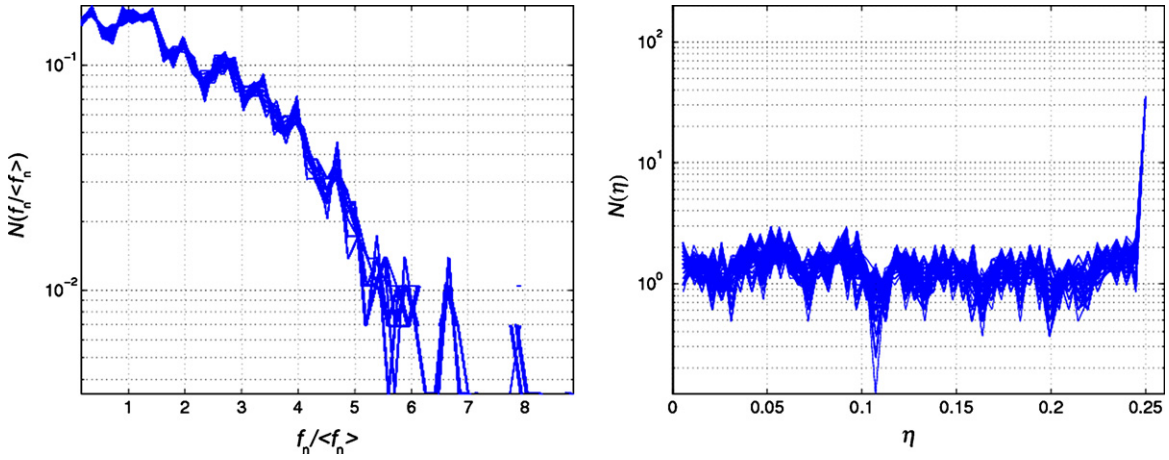

Fig. 10. Distribution function of the normal forces (left) and mobilized angle (right) at the contacts. The distributions are calculated from different times during the ratcheting regime (time = Nt_0, where N = 1000, 1001, . . ., 1500). The frequency distributions are constructed by segmenting the range of the data into 100 equally sized bins.

of sliding contacts per particle whose normal force is oriented between φ and $\varphi + \Delta\varphi$.

Samples compressed with zero deviatoric load are characterized by an isotropic distribution of sliding contacts. However, this isotropy is broken when the sample is subjected to the slightest deviatoric load. This appearance of the anisotropy can be schematically explained from Fig. 8. Let us assume that the contact force satisfies the sliding condition $|\vec{f}_t| = \mu|\vec{f}_n|$. Imagine that a small loading is imposed on the assembly in the vertical direction. If the normal component of the force is parallel to the loading direction, this component tends to increase more than the tangential force, so that the contact is likely to leave the sliding condition. On the contrary, if the tangential force is parallel to the loading direction it increases more than the normal force, and the contact is likely to remain in the sliding condition.

This picture is useful for explaining the complex evolution of the orientational distribution of the sliding contacts shown in Fig. 11. During the first cycle, sliding contacts whose normal force is oriented nearly parallel to the load direction leave the sliding condition during the loading phase, and some of them slip during the unload phase. On the other hand, the sliding contacts whose normal force is orientated nearly perpendicular to the load direction slip during the loading phase, and leave the sliding condition during the unload phase. In the first approximation, the anisotropy can be given by

$$\Omega^s(\varphi) \approx \begin{cases} \dfrac{N_0 n_s}{2\pi}(1 - \cos(2\varphi)) : \text{loading phase}, \\ \dfrac{N_0 n_s}{2\pi}(1 - \sin(2\varphi)) : \text{unloading phase}, \end{cases} \tag{7}$$

where $N_0 \approx 4.4$ is the averaged number of coordination number and n_s the fraction of sliding contacts. This description uses a single fabric coefficient n_s, which is accurate for intermediate loading amplitudes. For small loads the approximation is questionable due to the scarce number of sliding contacts. For large loads, a significant number of contacts reach the sliding contacts in both the load and unload phase, so that higher order fabric coefficients are required (Alonso-Marroquin & Herrmann, 2005). However, n_s can be considered as the most important internal variable describing the cyclic loading response.

The time evolution of n_s during cyclic loading is shown in Fig. 12. The relevance of this variable is demonstrated if one compares it with the evolution of the stiffness of the material. The latter is given by the slope of the stress strain curve in Fig. 5(a). During each loading phase, the number of sliding contacts increases, giving rise to a continuous decrease of the stiffness as shown in Fig. 5(a). The abrupt reduction in the number of sliding contacts at the transition from load to unload is reflected by the typical discontinuity in the stiffness observed under reversal loading. During cyclic loading the number of sliding contacts tends to decrease, which produces a narrowing of the hysteresis loops. In the long time behavior one can also see that some contacts reach almost periodically the sliding state even for extremely small loading cycles, leading to a constant amount of plastic deformation per cycle. Note also that the num-

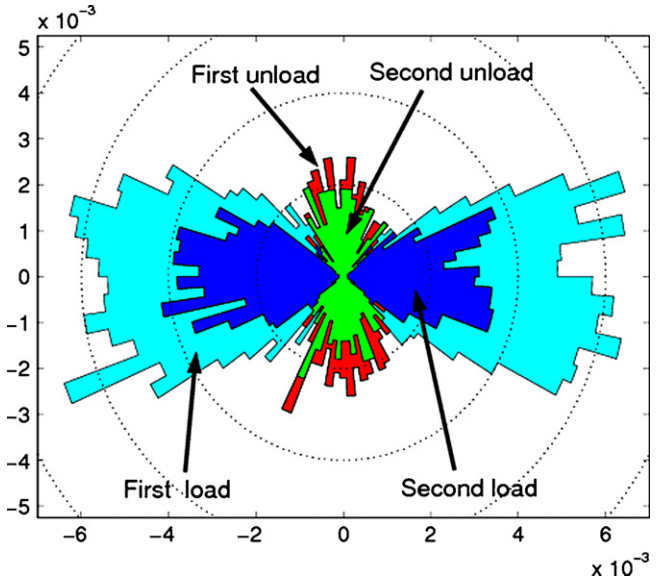

Fig. 11. Distribution of the orientation φ of the contacts reaching the sliding condition during the first two load–unload phases.

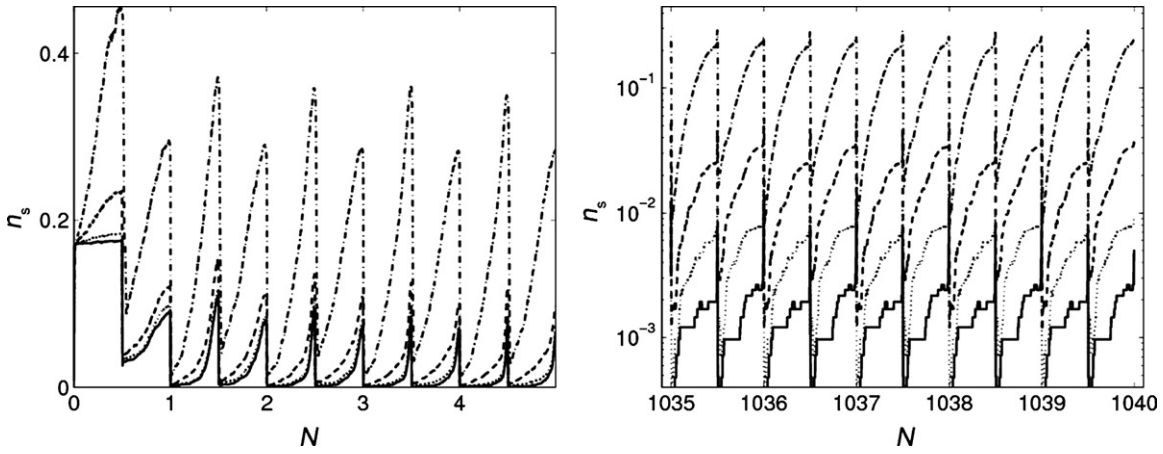

Fig. 12. Fraction of sliding contacts n_s in the short (left) and long time (right) behavior for different values of $\Delta\sigma_y/p_0$: 0.424 (dash-dotted line), 0.0707 (dashed line), 0.00707 (dotted line) and 0.000707 (solid line) (Alonso-Marroquin & Herrmann, 2004).

ber of contacts reaching the sliding conditions is almost the same in both loading and unloading phase. This makes the hysteresis loop almost symmetric, but slightly open to allow accumulation of plastic deformation.

At the contact level, the constant plastic deformation per cycle is explained from the variation of both force and displacement at the contacts. Fig. 13(a) and (c) shows the trajectories of the normal and tangential components of the force for two sliding contacts. After a certain number of loading cycles, the contact forces reach a periodic regime, some of them reaching periodically the sliding condition. The load–unload asymmetry of the contact force loop produces a slip at the contact of the same amount and in the same direction during each loading cycle.

A measure for the plastic deformation of the sliding contact is given by $\xi = (\Delta x_t^c - \Delta x_t^e)/\ell$, where Δx_t^c and Δx_t^e are the total and the elastic part of the tangential displacement at the contact. Fig. 13(b) and (d) shows the plastic deformation ξ of the two sliding contacts. Due to the load–unload asymmetry of the contact force loop, a net accumulation of plastic deformation is observed in each cycle. In the case of the contact shown in Fig. 13(b), the contact slips forward during the loading, and backward during the unloading phase. This sliding results in a net accumulation of permanent deformation per cycle. The other contact behaves elastically during the loading and slips during the unloading. This mechanism resembles the ratchets devices presented in Section 1.1. That is why this phenomenon is called granular ratcheting.

4.3. Displacement field

During the ratcheting regime, there is a constant accumulation of plastic deformation per cycle at each one of the sliding

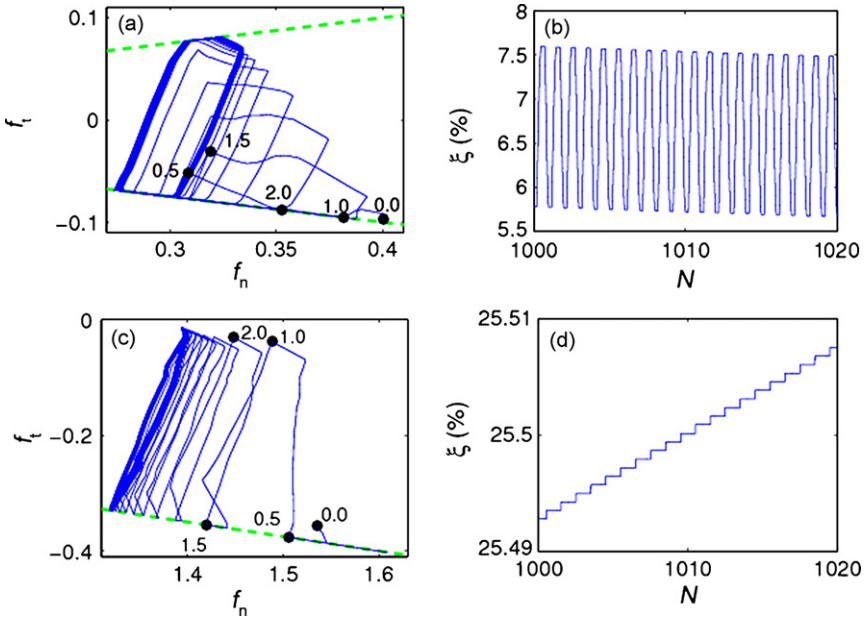

Fig. 13. (a) and (c) Trajectories of the contact force of two selected sliding contacts. The dots denote the times $t = 0, 0.5\,t_0, \ldots, 2\,t_0$, where t_0 is the period of the cyclic loading. The dashed line shows the sliding condition $|\vec{f}_t| = \mu|\vec{f}_n|$. (b) and (d) Plastic deformation ξ at the contacts shown in (a) and (c).

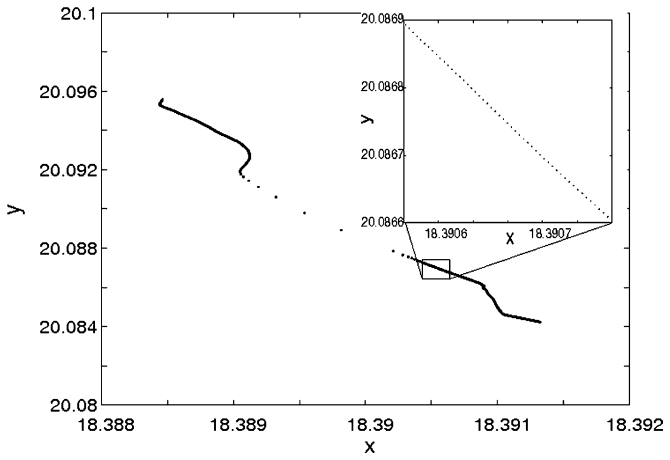

Fig. 14. Position of a single particle after each cycle. The detail shows the displacement during the ratcheting regime.

contacts. An immediate consequence of this fact is that each particle within the packing has a certain displacement and accumulates the same rotation for each cycle. The typical displacement of one particle during the cyclic loading is shown in Fig. 14. During the ratcheting regime, the particle moves the same amount in each cycle. This displacement remains constant during the long time of a ratcheting regime, but it changes abruptly during the transition between two ratcheting regimes. Typically, the maximal displacement per cycle at this transition is one or two orders of magnitude larger than in the ratcheting regimes. Therefore most of the deformation in the granular assembly occurs during the transitions. Deformation during ratcheting is relative small, but is sufficient to drive the system to unstable stages with relative large deformation.

It is interesting to observe the spatial correlation of such particle displacements. The most interesting deformation patterns is the formation of vorticity cells, see Fig. 15. Slow vorticity motion appears during the ratcheting regime, and fast motion vortices appear during the transition between two ratcheting regimes. This explains the evolution of the vorticity shown in Fig. 5(c), as well as the abrupt changes of vorticity shown in Fig. 5(f). Vortex structures are created and destroyed during the transitions. Therefore the vorticity patterns in each ratcheting regime are completely different from the previous one.

Since the vorticity is linked with a non-vanishing antisymmetric part of the displacement gradient, the strain tensor is not sufficient to provide a complete description of this convective motion during cyclic loading. Slip zones and rotational bearings are other persistent deformation patterns during the cyclic loading (Alonso-Marroquin & Herrmann, 2004; García-Rojo et al., 2005). They appear periodically during each ratcheting regime. Patterns are destroyed and new ones are created during the transition between two ratcheting regimes. An appropriate constitutive model for ratcheting demands additional degrees of freedom in the continuum, taking into account these deformation patterns in strain-like variables.

5. Concluding remarks

A grain scale investigation of the cyclic loading response of a packing of polygons has been presented. In the quasistatic limit, we have shown the existence of long time regimes with a constant accumulation of plastic deformation per cycle, due to ratchet-like motion at the sliding contacts. As the loading amplitude decreases, a smooth transition from ratcheting to shakedown is observed, which does not allow one to identify a purely elastic regime.

The overall response of the polygonal packing under cyclic loading consists of a sequence of long time ratcheting regimes, with slow accumulation of plastic deformation in terms of deviatoric strains, compaction and vorticity. These regimes are separated by short time regimes with large plastic deformations.

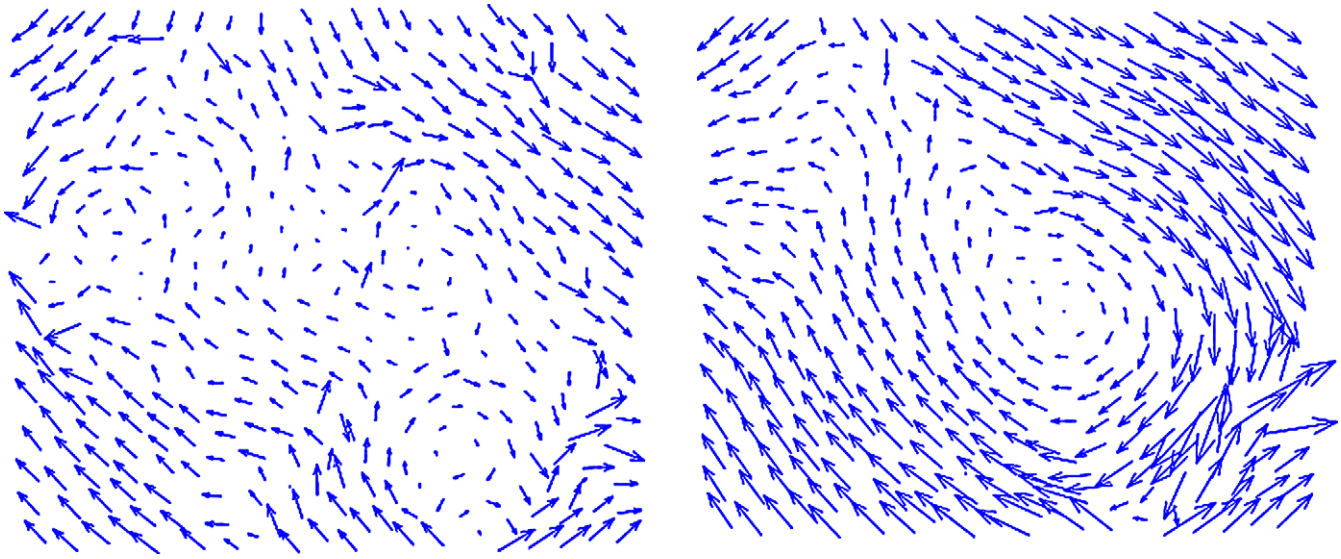

Fig. 15. Displacement field during one loading cycle. The load amplitude is $\Delta\sigma = 0.6\,p_0$, and $p_0 = 0.001\,k_n$. The left image corresponds to the displacement per cycle during the ratcheting regime; the right one is the displacement per cycle during the transition between two ratcheting regimes. The arrows represent $10^5\,\Delta\vec{u}$ in the left image and $10^3\,\Delta\vec{u}$ in the right one, where $\Delta\vec{u}$ is the displacement of the particle per cycle.

The analysis of the displacement field per cycle of the particles shows that cyclic loading induce convective motion inside the sample. This motion appears in form of vortex-like structures, which persist during the ratcheting regime.

The existence of granular ratcheting may have deep implications in the study of permanent deformation of geomaterials subject to cyclic loading. More precisely, the classical concept of an elastic regime needs to be abandoned, because any load induces irreversible deformation. A continuum description of ratcheting requires the introduction of additional degrees of freedom in the kinematics, as well as internal variables in the constitutive relations. These internal variables must account for the dissipation produced by the sliding contacts in the ratcheting regime, and the restructuring of the granular skeleton during the transition between two ratcheting regimes. Recently two approaches have been suggested to this issue. They extrapolate the statistical mechanics of viscoelastic fluids (Jiang & Liu, 2007) and thermally activated dislocations (Gudehus, 2006b, 2008) to jammed granular materials. These approaches introduce two different temperatures as internal variables, accounting for frictional dissipation and energy released by unjammed transitions. The validity of these approaches remains conditioned to the validation of the ergodic hypothesis for jammed granular media.

Geotechnical application of cyclic loading simulations is still limited by the computer time needed for simulations. However, simulations of thousands of cycles with small number of particles can be used to investigate the microscopic origin of granular ratcheting, which will contribute to the development of large scale simulation models. At this time, the similarity of results with the recently reported ratcheting regime in packings of disks (García-Rojo et al., 2005) and spheres (David et al., 2005) indicates that this effect does not depend on the geometry of the grains, and that it may be inherent to the particle interactions.

Modeling interactions between polygons still poses serious limitations, because of the difficulty to derive conservative elastic forces: when forces between polygons are calculated as a function of their overlapping area, the energy conservation is not guaranteed (Poeschel & Schwager, 2004). An alternative approach is to define the potential energy as a function of overlap, and derive from this potential contact forces and torques (Poeschel & Schwager, 2004). However, this approach leads to unrealistic interactions, because the magnitudes of the torque applied to each particle are the same. Moreover, the derivation of forces from this potential leads to complicated expressions which are difficult to code. A simpler approach has been proposed, where a potential energy is associated to each vertex–edge interaction between the polygons (Alonso-Marroquin, 2008). McNamara, García-Rojo, & Herrmann (2008) show further difficulties when the classical Cundall–Strack frictional force is used in simulations of packing of disks. This force leads to path dependency in the potential energy, even when sliding is hindered in the simulations. They also show that an alternative method for calculating tangential forces in packing of disks removes granular ratcheting. Thus, future modeling of cyclic loading needs to develop more realistic normal and tangential contact force laws, and to understand the relation between the contact model and the onset of permanent deformations.

Acknowledgements

F. Alonso-Marroquin is the recipient of an Australian Research Council Postdoctoral Fellowship (project number DP0772409), and acknowledges the support of the ALERT Geomaterials Prize 2006. The authors thank S. McNamara for discussions, and G. Gudehus for helpful written communications.

References

Allen, M. P., & Tildesley, D. J. (1987). *Computer simulation of liquids*. Oxford: Oxford University Press.

Alonso-Marroquin, F. (2004). Micromechanical investigation of soil deformation: Incremental response and granular ratcheting. Doctoral Dissertation, University of Stuttgart, Logos Verlag Berlin, ISBN 3-8325-0560-1.

Alonso-Marroquin, F., & Herrmann, H. J. (2002). Calculation of the incremental stress–strain relation of a polygonal packing. *Physical Review E*, *66*, 021301.

Alonso-Marroquin, F., & Herrmann, H. J. (2004). Ratcheting of granular materials. *Physical Review Letters*, *92*(5), 054301.

Alonso-Marroquin, F., & Herrmann, H. (2005). Investigation of the incremental response of soils using a discrete element model. *Journal of Engineering Mathematics*, *52*, 11–34.

Alonso-Marroquin, F., Luding, S., Herrmann, H., & Vardoulakis, I. (2005). Role of anisotropy in the elastoplastic response of a polygonal packing. *Physical Review E*, *71*, 051304.

Alonso-Marroquin, F., Vardoulakis, I., Herrmann, H. J., Weatherley, D., & Mora, P. (2006). Effect of rolling on dissipation in fault gouges. *Physical Review E*, *74*, 031306.

Alonso-Marroquin, F. (2008). Spheropolygons: A new method to simulate conservative and dissipative interactions between 2D complex-shaped rigid bodies. *Europhysics Letters*, *83*(1), 14001.

Bardet, J. P. (1994). Numerical simulations of the incremental responses of idealized granular materials. *International Journal of Plasticity*, *10*, 879–908.

Burland, J., & Viggiani, C. (1994). Observazioni sul comportamento della torre di pisa. *Rivista Italiana di Geotecnica*, *28*(3), 179–200.

Calvetti, F., Viggiani, G., & Tamagnini, C. (2003). *Micromechanical inspection of constitutive modeling. Constitutive modelling and analysis of boundary value problems in Geotechnical Engineering*. Benevento: Hevelius Edizioni., pp. 187–216.

Chambon, R., Desrues, J., Hammad, W., & Charlier, R. (1994). CLoE, a new rate-type constitutive model for geomaterials: Theoretical basis and implementation. *International Journal for Numerical and Analytical Methods in Geomechanics*, *18*, 253–278.

Cundall, P. A., & Strack, O. D. L. (1979). A discrete numerical model for granular assemblages. *Geotechnique*, *29*, 47–65.

Dafalias, Y. F. (1986). Bounding surface plasticity. I. Mathematical foundation and hypoplasticity. *Journal of Engineering Mechanics*, *112*(9), 966–987.

Darve, F., Flavigny, E., & Meghachou, M. (1995). Yield surfaces and principle of superposition: Revisit through incrementally non-linear constitutive relations. *International Journal of Plasticity*, *11*(8), 927.

David, C. T., García-Rojo, R., Herrmann, H. J., & Luding, S. (2005). Hysteresis and creep in powders and grains. In R. Garcia-Rojo, H. Herrmann, & S. McNamara (Eds.), *Proceedings of Powders and Grains* (pp. 291–294). Leiden: Balkema.

Dybvig, P. H. (1995). Dusenberry's ratcheting of consumption: Optimal dynamic consumption and investment given intolerance for any decline in standard of living. *The Review of Economic Studies*, *62*(2), 287–313.

England, G. L., Tsang, T. D. C. M., Mihajlovic, N., & Bazaz, J. B. (1995). Ratcheting flow of granular materials. In M. D. Evans & R. J. Fragaszy (Eds.), *Static and dynamic properties of gravelly soils*. ASCE, pp. 64-76.

Festag, G. (2003). Experimental investigation on sand under cyclic loading. In *Constitutive and centrifuge modelling: two extremes*. Monte Verita, pp. 269–277.

Feynman, R. P., Leighton, R. B., & Sands, M. (1963). *The Feynman lectures on physics (Vol. 1)* Massachusetts: Addison Wesley., pp. 46.1–46.9, Chapter 46.

Garcia-Rojo, R., & Herrmann, H. J. (2005). Shakedown of unbound granular materials. *Granular Matter*, *7*(2), 109–118.

García-Rojo, R., Alonso-Marroquin, F., & Herrmann, H. J. (2005). Characterization of the material response in the granular ratcheting. *Physical Review E*, *72*, 041302.

Gudehus, G. (1979). A comparison of some constitutive laws for soils under radially symmetric loading and unloading. *Canadian Geotechnical Journal*, *20*, 502–516.

Gudehus, G. (2006a). Seismo-hypoplasticity with a granular temperature. *Granular Matter*, *8*, 93–102.

Gudehus, G. (2006b). Seismo-hypoplasticity state limits of granular skeletons. *Journal of Statistical Mechanics*, *7*, P07022.

Gudehus, G. (2008). *Physical soil mechanics*. Berlin: Springer., ISBN 978-3-540-36353-8. Chapter 4.9.

Gudehus, G., Darve, F., & Vardoulakis, I. (1984). *Constitutive relations of soils*. Rotterdam: Balkema.

Hashiguchi, K., & Chen, Z. P. (1998). Elastoplastic constitutive equation of soil with the subloading surface and rotational hardening. *International Journal for Numerical and Analytical Methods in Geomechanics*, *22*, 197–227.

Howard, J. (1997). Molecular motors: Structural adaptation to cellular functions. *Nature*, *389*, 561–567.

Huang, M., Suo, Z., Ma, Q., & Fujimoto, H. (2000). Thin film cracking and ratcheting caused by temperature cycling. *Journal of Materials Research*, *15*(6), 1239–1242.

Jiang, Y., & Liu, M. (2007). From elasticity to hypoplasticity: Dynamics of granular solids. *Physical Review Letters*, *99*(10), 105501.

Kishino, Y. (2003). On the incremental nonlinearity observed in a numerical model for granular media. *Italian Geotechnical Journal*, *3*, 3–12.

Kitamura, K., Tokunaga, K., Iwane, M., & Yanagida, T. (1999). A single myosin head moves along an actin filament with regular steps of 5.3 nanometres. *Nature*, *397*(6715), 129–134.

Kolymbas, D. (1993). *Modern approaches to plasticity*. Amsterdam: Elsevier Sciences Publishers.

Kolymbas, D., Herle, I., & Wolfferdorff, P. A. (1995). A hypoplastic constitutive equation with back stress. *International Journal for Numerical and Analytical Methods in Geomechanics*, *19*, 415–446.

Kun, F., & Herrmann, H. J. (1999). Transition from damage to fragmentation in collision of solids. *Physical Review E*, *59*(3), 2623–2632.

Lekarp, F., & Dawson, A. (1998). Modelling permanent deformation behaviour of unbound granular materials. *Construction and Building Materials*, *12*(1), 9–18.

Lekarp, F., Dawson, A., & Isacsson, U. (2000). Permanent strain response of unbound aggregates. *Journal of Transportation Engineering ASCE*, *126*(1), 76–82.

Lobo-Guerrero, S., & Vallejo, L. E. (2006). Discrete element method analysis of railtrack ballast degradation during cyclic loading. *Granular Matter*, *8*(3–4), 195–204.

Luding, S. (2004). Micro-macro transition for anisotropic, frictional granular packings. *International Journal of Solids and Structures*, *41*, 5821–5836.

Madadi, M., Tsoungui, O., Lätzel, M., & Luding, S. (2004). On the fabric tensor of polydisperse granular media in 2D. *International Journal of Solids and Structures*, *41*(9–10), 2563–2580.

Majmudar, T. S., & Behringer, R. P. (2005). Contact force measurements and stress-induced anisotropy in granular materials. *Nature*, *435*, 47–61.

McNamara, S., García-Rojo, R., & Herrmann, H. (2008). Microscopic origin of granular ratcheting. *Physical Review E*, *77*(3), 31304.

Niemunis, A., & Herle, I. (1997). Hypoplastic model for cohesionless soils with elastic strain range. *Mechanics of Cohesive-Frictional Material*, *2*, 279–299.

Nova, R., & Wood, D. (1979). A constitutive model for sand in triaxial compression. *International Journal for Numerical and Analytical Methods in Geomechanics*, *3*, 277–299.

Peña, A. A., Lizcano, A., Alonso-Marroquin, F., & Herrmann, H. J. (2005). Investigation of the asymptotic states of granular materials using a discrete model of anisotropic particles. In *Proceedings of Powders and Grains, vol. 1* (pp. 697–700).

Pena, A., Lizcano, A., Alonso-Marroquin, F., & Herrmann, H. J. (2008). Biaxial test simulations using a packing of polygonal particles. *International Journal for Numerical and Analytical Methods in Geomechanics*, *32*(2), 143–160.

Poeschel, T., & Schwager, T. (2004). *Computational granular dynamics*. Berlin: Springer.

Poorooshasb, H. B., Holubec, I., & Sherbourne, A. N. (1967). Yielding and flow of sand in triaxial compression. *Canadian Geotechnical Journal*, *4*(4), 376–397.

Reimann, P. (2002). Brownian motors: Noisy transport far from equilibrium. *Physics Reports*, *361*, 57–265.

Roscoe, K. H., & Burland, J. B. (1968). On the generalized stress-strain behavior of 'wet' clay. In *Engineering plasticity*. Cambridge: Cambridge University Press., pp. 535–609.

Royer-Carfagni, G. (2004). *Granular decohesion thermal damage in marble monuments. Novel approaches in civil engineering*. Berlin: Springer-Verlag., pp. 177–185.

Sharp, R. W., & Booker, J. R. (1984). Shakedown of pavements under moving surface loads. *Journal of Transportation Engineering*, *110*, 1–14.

Svoboda, K., Schmidt, C. F., Schnapp, B. J., & Block, S. M. (1993). Direct observation of kinesin stepping by optical trapping interferometry. *Nature*, *365*(6448), 721–727.

Tillemans, H. J., & Herrmann, H. J. (1995). Simulating deformations of granular solids under shear. *Physica A*, *217*, 261–288.

Triantafyllidis, T. (Ed.). (2004). *Cyclic behaviour of soils and liquefaction phenomena*. Leiden: A.A. Balkema Publishers.

Vardoulakis, I. (1983). Rigid granular plasticity model and bifurcation in the triaxial test. *Acta Mechanica*, *49*, 57–79.

Vardoulakis, I., & Georgopoulos, I. O. (2005). The stress–dilatancy hypothesis revisited: Shear-banding related instabilities. *Soils & Foundations*, *45*, 61–76.

Vermeer, P. A. (1984). *A five-constant model unifying well-established concepts. Constitutive relations of soils*. Rotterdam: Balkema., pp. 175–197.

Werkmeister, S., Dawson, A. R., & Wellner, F. (2001). Permanent deformation behavior of granular materials and the shakedown theory. *Journal of Transportation Research Board*, *1757*, 75–81.

Werkmeister, S., Numrich, R., Dawson, A. R., & Wellner, F. (2002). *Deformation behaviour of granular material under repeated dynamic loading. Environmental Geomechanics*. Monte Verita: Presses Polytechniques et Universitaires Romandes.

Wood, D. M. (1990). *Soil behaviour and critical state soil mechanics*, Cambridge, ISBN 0-521-33782-8.

Zapata, I., Bartussek, R., Sols, F., & Hänggi, P. (1996). Voltage rectification by a squid ratchet. *Physical Review Letters*, *77*(11), 2292–2295.